Abrogation of prenucleation, transient oligomerization of the Huntingtin exon 1 protein by human profilin I

Alberto Ceccon[a], Vitali Tugarinov[a,1], Rodolfo Ghirlando[b], and G. Marius Clore[a,1]

[a]Laboratory of Chemical Physics, National Institute of Diabetes and Digestive and Kidney Diseases, National Institutes of Health, Bethesda, MD 20892-0520; and [b]Laboratory of Molecular Biology, National Institute of Diabetes and Digestive and Kidney Diseases, National Institutes of Health, Bethesda, MD 20892-0540

Contributed by G. Marius Clore, January 28, 2020 (sent for review December 19, 2019; reviewed by Lewis E. Kay and David J. Weber)

Human profilin I reduces aggregation and concomitant toxicity of the polyglutamine-containing N-terminal region of the huntingtin protein encoded by exon 1 (htt^{ex1}) and responsible for Huntington's disease. Here, we investigate the interaction of profilin with htt^{ex1} using NMR techniques designed to quantitatively analyze the kinetics and equilibria of chemical exchange at atomic resolution, including relaxation dispersion, exchange-induced shifts, and lifetime line broadening. We first show that the presence of two polyproline tracts in htt^{ex1}, absent from a shorter huntingtin variant studied previously, modulates the kinetics of the transient branched oligomerization pathway that precedes nucleation, resulting in an increase in the populations of the on-pathway helical coiled-coil dimeric and tetrameric species ($\tau_{ex} \leq 50$ to 70 μs), while leaving the population of the off-pathway (nonproductive) dimeric species largely unaffected (τ_{ex} ∼750 μs). Next, we show that the affinity of a single molecule of profilin to the polyproline tracts is in the micromolar range ($K_{diss} \sim 17$ and ∼ 31 μM), but binding of a second molecule of profilin is negatively cooperative, with the affinity reduced ∼11-fold. The lifetime of a 1:1 complex of htt^{ex1} with profilin, determined using a shorter huntingtin variant containing only a single polyproline tract, is shown to be on the submillisecond timescale ($\tau_{ex} \sim 600$ μs and $K_{diss} \sim 50$ μM). Finally, we demonstrate that, in stable profilin–htt^{ex1} complexes, the productive oligomerization pathway, leading to the formation of helical coiled-coil htt^{ex1} tetramers, is completely abolished, and only the pathway resulting in "nonproductive" dimers remains active, thereby providing a mechanistic basis for how profilin reduces aggregation and toxicity of htt^{ex1}.

relaxation-based NMR | short-lived excited states | oligomerization | binding kinetics | negative cooperativity

Huntington's disease is a fatal, autosomal-dominant, neurodegenerative condition arising from expansion of the polyglutamine (polyQ) tract beyond 35 repeats within exon 1 of the huntingtin (*HTT*) gene (1, 2). Proteolysis (3) or incomplete mRNA splicing of the *HTT* gene (4) results in pathogenic mutated N-terminal fragments encoded by exon 1 (5) that self-associate into polymorphic aggregates of oligomers and fibers (6, 7) to form neuronal inclusion bodies (8). The polypeptide encoded by exon 1, htt^{ex1}, comprises three domains: a 16-residue N-terminal amphiphilic sequence (NT domain), a polyQ tract of variable length, and a proline-rich domain (PRD) comprising two polyproline repeats (P_{11} and P_{10}) separated by a 17-residue linker.

From a structural perspective, htt^{ex1} assembles into fibrils consisting of a polyQ β-hairpin core surrounded by the NT and PRD domains that retain a significant degree of inherent mobility (9–12). The kinetics of aggregation is modulated by the regions on either side of the polyQ tract: The NT domain promotes fibril formation, while the PRD reduces aggregation propensity (9, 11, 13–15). Additional factors affecting aggregation include interaction of the NT domain with lipid membranes (16), posttranslational modifications (17–19), and binding to various ligands (20, 21). In this regard, human profilin I, a ubiquitous eukaryotic protein that binds actin, poly-L-proline, and phosphatidylinositol 4,5-biphosphate (22), has been shown to significantly reduce aggregation and toxicity of htt^{ex1} (23, 24) by binding to the PRD (25).

Recently, we investigated the transient (submillisecond) prenucleation events involved in the early stages of oligomerization of a minimalistic construct of htt^{ex1} ($htt^{NT}Q_7$) comprising the NT and polyQ domains but lacking the PRD (26). Using relaxation-based NMR measurements, we were able to show that oligomerization of the N-terminal domain of $htt^{NT}Q_7$ involves a branched pathway: one (on-pathway) leading to a "productive" helical coiled-coil dimer that further self-associates into a tetramer (comprising a dimer of dimers), and the other (off-pathway) leading to a "nonproductive," partially helical dimer (or ensemble of dimers) that does not undergo further oligomerization. Here, using NMR, we investigate the effects of human profilin I on the oligomerization of the full-length exon 1 Huntingtin protein, htt^{ex1}. We first show that the branched oligomerization pathway is preserved in the presence of the PRD. Next, we show that profilin binds specifically to the two polyproline tracts (P_{11} and P_{10}) within the PRD, and quantitatively characterize the binding equilibria involved, as well as the lifetime of a 1:1 complex. Finally, we show that binding

Significance

Polyglutamine expansion within the N-terminal region of huntingtin encoded by exon 1 (htt^{ex1}) results in accumulation of htt^{ex1} aggregates in neurons, leading to Huntington's disease. Profilin is a ubiquitous intracellular protein that reduces aggregation and toxicity of htt^{ex1}. Prenucleation, transient oligomerization of the htt^{ex1} N-terminal amphiphilic domain proceeds along two branches: an on-pathway, "productive" branch resulting in a helical coiled-coil tetramer that supports nucleation of the polyglutamine tract and subsequent aggregation, and an off-pathway "nonproductive" branch that does not proceed beyond a partially helical dimer. Using NMR, we show that profilin binding to the proline-rich domain of htt^{ex1} blocks the on-pathway oligomerization pathway while leaving the off-pathway branch unaffected, thereby providing a mechanistic basis for profilin inhibition of htt^{ex1} aggregation.

Author contributions: A.C., V.T., and G.M.C. designed research; A.C., V.T., R.G., and G.M.C. performed research; A.C., V.T., and G.M.C. analyzed data; and A.C., V.T., and G.M.C. wrote the paper.

Reviewers: L.E.K., University of Toronto; and D.J.W., University of Maryland, Baltimore.

The authors declare no competing interest.

Data deposition: The backbone chemical shifts of htt^{ex1} reported in this paper have been deposited in the Biological Magnetic Resonance Data Bank (BMRB), http://www.bmrb.wisc.edu (accession no. 50122). The experimental data in digital format, together with MatLab scripts used in global fitting, have been deposited on Figshare (DOI: 10.6084/m9.figshare.11887860). Note that the backbone assignments are explicitly indicated on the ^{1}H–^{15}N correlation spectrum shown in Fig. 1. There are no atomic coordinates or structural restraints associated with the current submission.

[1]To whom correspondence may be addressed. Email: mariusc@mail.nih.gov or vitali.tugarinov@nih.gov.

This article contains supporting information online at https://www.pnas.org/lookup/suppl/doi:10.1073/pnas.1922264117/-/DCSupplemental.

First published March 3, 2020.

of profilin completely abrogates the productive oligomerization pathway that leads to the helical coiled-coil tetramer, while leaving the nonproductive pathway, which does not extend beyond a dimer, unaffected. These results provide a molecular basis for the mechanism whereby profilin binding reduces the aggregation propensity and toxicity of htt^{ex1}.

Results and Discussion

Impact of the PRD Domain on the Kinetics of Transient htt^{ex1} Oligomerization. The domain architecture of the 73-residue htt^{ex1} construct used in the present work is shown in Fig. 1*A*. The PRD domain comprises two polyproline tracts, P_{11} and P_{10}, separated by a 17-residue linker and followed by a 12-residue C-terminal sequence. In the current work, we have chosen to keep the length of the polyQ tract at seven glutamines to both facilitate comparison with our earlier work on $htt^{NT}Q_7$ (26), as well as to ensure that the construct remains largely monomeric and stable during the course of the NMR experiments (several weeks). Sedimentation velocity experiments (*SI Appendix*, Fig. S1) confirm that the major, directly observable species of htt^{ex1} is monomeric (with a single peak at 0.74 S corresponding to an estimated mass of 7.9 kDa). The ^1H–^{15}N heteronuclear single quantum coherence (HSQC) spectrum of htt^{ex1} exhibits very limited ^1H chemical shift dispersion (Fig. 1*B*) characteristic of an intrinsically disordered polypeptide.

Quantitative characterization of the transient prenucleation oligomerization events involving the submillisecond interconversion between monomeric and sparsely populated multimeric species of htt^{ex1} was probed using the same experimental approach and data analysis employed previously for $htt^{NT}Q_7$ (26). The experimental data comprised ^{15}N and $^{13}C\alpha$ Carr–Purcell–Meiboom–Gill (CPMG) relaxation dispersions (27, 28) at three concentrations (0.3, 0.6, and 0.8 mM), and ^{15}N and $^{13}C\alpha$ exchange-induced shifts (δ_{ex}) (29) at 12 concentrations ranging from 50 μM to 1.2 mM (Fig. 2 *A* and *B* and *SI Appendix*, Fig. S2). The NMR data were analyzed simultaneously within the framework of the branched kinetic scheme shown in Fig. 2*C*, which features on-pathway (productive) and off-pathway (nonproductive) self-association branches. The major observable species is the monomeric state **E**. The on-pathway pathway leads to the formation of an excited state tetramer $\mathbf{E_4}$ via the productive dimer $\mathbf{E_2}$. (Note that direct conversion of monomer to tetramer is not only physically unrealistic but leads to a steeper concentration dependence of δ_{ex}.) In the case of the off-pathway branch, the resulting dimer $\mathbf{E_2^*}$ represents an "end state" that does not undergo further oligomerization. Details of the kinetic model, and data fitting procedures, as well as the assumptions and approximations used in the data analysis, are provided in *SI Appendix*.

The $^{13}C\alpha$ and ^{15}N chemical shift differences (*SI Appendix*, Table S1) between the monomer and the on-pathway dimer and tetramer (which are assumed to be the same) are fully consistent with the formation of a helical coiled-coil comprising residues 3 to 16 of the NT domain, while those between the monomer and off-pathway dimer are consistent with the formation of an ensemble of partially helical states of the NT domain, as described previously for $htt^{NT}Q_7$ (26). The overall interconversion between **E** and $\mathbf{E_4}$ is fast on the chemical shift timescale ($\tau_{ex} \leq 50$ to 70 μs; *SI Appendix*, Fig. S3) and tetramerization is responsible for the curvature of the concentration dependence of the $^{15}N/^{13}C\alpha$-δ_{ex} data (Fig. 2*B*). The off-pathway interconversion between **E** and $\mathbf{E_2^*}$ proceeds on a much slower timescale ($\tau_{ex} \sim 750$ μs). Both on- and off-pathway processes contribute to the CPMG relaxation dispersion data, with the contribution from the latter being suppressed at CPMG fields in excess of about 600 Hz; the contribution, however, of off-pathway dimerization to the concentration dependence of $^{15}N/^{13}C\alpha$-δ_{ex} is negligible (*SI Appendix*, Fig. S4). No significant CPMG relaxation dispersions or concentration-dependent changes in $^{15}N/^{13}C\alpha$-δ_{ex} values are observed beyond the $polyQ_7$ tract (*SI Appendix*, Figs. S5 and S6), indicating that the PRD does not participate directly in the intermolecular interactions that drive the transient, prenucleation oligomerization events.

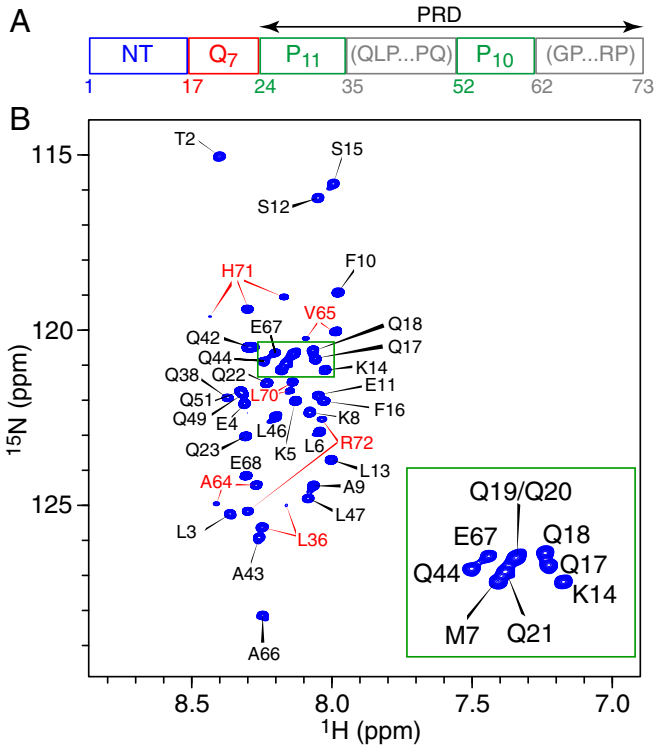

Fig. 1. Domain organization and NMR characterization of htt^{ex1}. (*A*) Schematic representation of the domain architecture of the htt^{ex1} construct used in the current study. (*B*) ^1H–^{15}N HSQC spectrum of htt^{ex1} (600 MHz; 5 °C). The portion of the spectrum enclosed in the green box is zoomed in the *Bottom Right* corner of the figure. Cross-peaks are labeled with the assigned residue numbers in black, except for residues labeled in red that display additional cross-peaks as a result of proximity to at least one proline undergoing *cis*/*trans* isomerization that is slow on the chemical shift timescale. These residues are located either in the linker connecting the two polyproline tracts (Leu36) or in the region C-terminal to the second polyproline tract (Ala64, Val65, Leu70, His71, and Arg72). The additional cross-peaks are much weaker than the main correlations and constitute less than 5% of the total intensity, in agreement with similar observations on other unfolded proteins (37). Three correlations are observed for His71, which is proximal to two proline residues at positions $i - 2$ and $i + 2$. Almost complete (97%) chemical shift assignments of ^{15}N, $^{13}C\alpha$, $^{13}C'$, and $^{13}C\beta$ nuclei of all nonproline residues of $^{15}N/^{13}C$-labeled htt^{ex1} were obtained using standard three-dimensional triple-resonance NMR experiments (*SI Appendix*, *Materials and Methods*).

The rate constants for the on- and off-pathway kinetic steps are broadly comparable (within a factor of ~2) to those observed for the shorter $htt^{NT}Q_7$ construct (26). However, at the highest concentration of 1.2 mM used in both studies, the populations of the on-pathway dimer ($\mathbf{E_2}$) and tetramer ($\mathbf{E_4}$) are significantly increased (~1.5- and ~2.5-fold, respectively) for htt^{ex1} relative to $htt^{NT}Q_7$, which is reflected in proportionately larger δ_{ex} values. Furthermore, the overall equilibrium dissociation constant of the tetramer into monomer, given by $K_1^{diss}K_2^{diss}$, is reduced by ~35% for htt^{ex1} (1.7 μM^2) relative to $htt^{NT}Q_7$ (2.6 μM^2). These findings might be explained by the presence of additional transient interactions between the NT and PRD domains and in the case of the tetramer between the PRD domains as well. The population of the off-pathway dimer $\mathbf{E_2^*}$, however, is the same for the two constructs (~1% at 1.2 mM).

Binding of Profilin to htt^{ex1}. The htt^{ex1} binding site on profilin I was delineated by $^1H_N/^{15}N$ chemical shift perturbation mapping in which the positions of cross-peaks in a series of ^1H–^{15}N HSQC

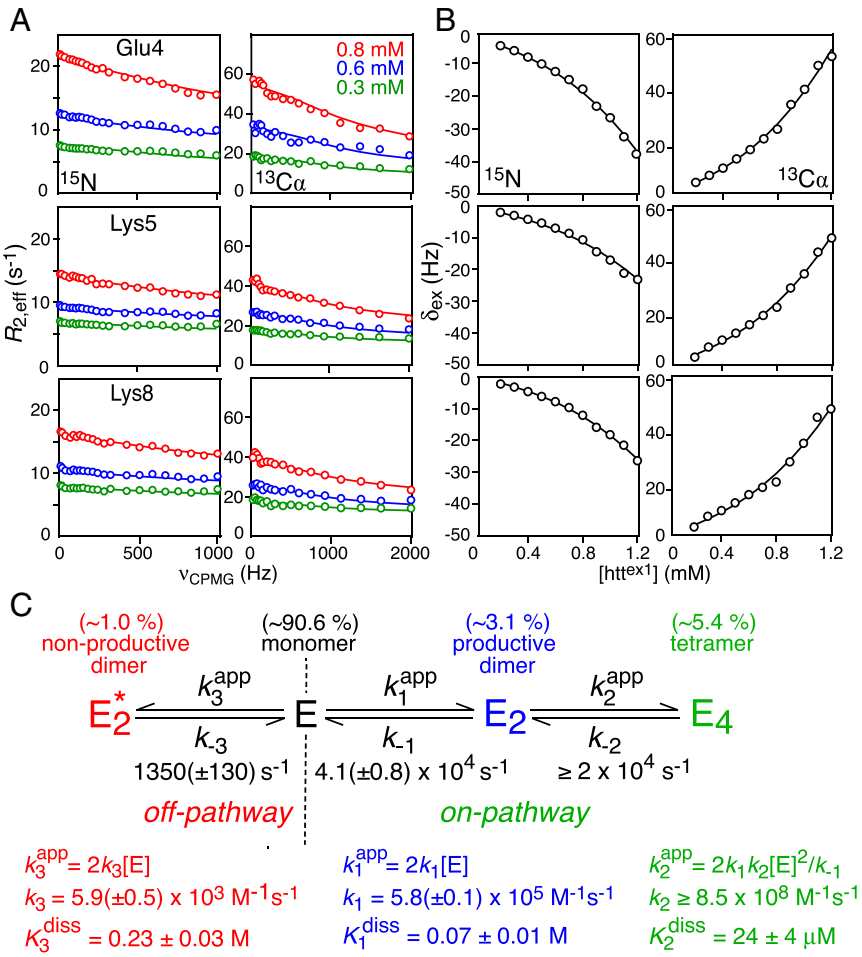

Fig. 2. Quantitative analysis of transient oligomerization of htt^{ex1}. Examples of (*A*) ^{15}N (*Left*) and ^{13}Cα (*Right*) CPMG relaxation dispersion profiles at three concentrations (0.3, 0.6, and 0.8 mM); and (*B*) ^{15}N (*Left*) and ^{13}Cα (*Right*) exchange-induced shifts (δ_{ex}) over concentrations ranging from 200 μM to 1.2 mM (referenced relative to the shifts at 50 μM htt^{ex1}). Experimental data, recorded at 900 MHz and 5 °C, are displayed as circles, and the best-fit curves obtained from a global fit to the kinetic scheme in *C* are shown as solid lines. (*C*) Minimal kinetic model for prenucleation transient oligomerization of htt^{ex1} that accounts for all of the experimental NMR data. The kinetic scheme comprises two branches: an on-pathway branch that leads to a helical coiled-coil tetramer ($\mathbf{E_4}$) via a "productive" coiled-coil helical dimer, $\mathbf{E_2}$; and an off-pathway branch that terminates in a "nonproductive" partially helical dimer, $\mathbf{E_2^*}$. The populations of the various species at [htt^{ex1}] = 1.2 mM, the highest concentration used in the NMR experiments, are provided above each state. The complete set of data used in the global fit is provided in *SI Appendix*, Fig. S2. For errors of 0.3 Hz and 0.6 s^{-1} for δ_{ex} and $R_{2,eff}$, respectively, the reduced χ^2 is 2.3.

spectra of ^{15}N-labeled profilin were monitored upon titration with unlabeled htt^{ex1}. A contiguous, predominantly hydrophobic, binding surface, characterized by $\Delta_{H/N}$ chemical shift perturbations in excess of 0.09 ppm upon addition of 0.9 mM htt^{ex1} to 0.4 mM profilin, is formed by the N-terminal end of helix α1 (residues 3 and 6), the C-terminal end of helix α3 (residues 130, 131, and 133 to 138) and the turns connecting strands β1 and β2 (residues 24 and 25) and strands β5 and β6 (residues 106 to 108) (Fig. 3*A*). The htt^{ex1} binding surface on profilin corresponds to that for poly-L-proline (23, 30, 31), and partially overlaps with the site of profilin self-association (helix α4) (32). However, at the concentration of profilin employed (0.4 mM), the population of dimeric and tetrameric states of profilin is insignificant (32).

$^{1}H_N/^{15}N$ chemical shift perturbation mapping of ^{15}N-labeled htt^{ex1} upon titration with unlabeled profilin reveals chemical shift perturbations for residues immediately adjacent to the N- and C-terminal ends of both polyproline tracts as well as residues between the two polyproline tracts (Fig. 3*B*). Furthermore, the ^{1}H–^{13}Cα cross-peaks for the two polyproline tracts are broadened out very early on during the course of the titration (Fig. 3*C*). Thus, one can conclude that profilin binds to the P_{11} and P_{10} polyproline repeats.

Quantitative Analysis of Profilin–htt^{ex1} Binding Equilibria. To obtain a quantitative description of the equilibria involving the binding of htt^{ex1} to profilin, we globally fit ^{15}N exchange-induced shift (^{15}N-δ_{ex}) data for 0.4 mM ^{15}N-labeled profilin upon titration with unlabeled htt^{ex1} (Fig. 4*A*), and ^{15}N-δ_{ex} and ^{15}N lifetime line broadening ($^{15}N - \Delta R_2^{1.5kHz}$) data for 0.1 mM ^{15}N-labeled htt^{ex1} upon titration with unlabeled profilin (Fig. 4*B*) to the minimalistic binding scheme depicted in Fig. 4*C* (see *SI Appendix* for details of the global fitting procedure). Under these experimental conditions, the populations of oligomeric htt^{ex1} species (Fig. 2) are sufficiently low to be neglected. Initially, a single molecule of profilin (**P**) binds to either one of the two polyproline tracts of htt^{ex1} (**E**) to form two possible singly occupied complexes, **PE** (profilin-P_{11}) and **PE′** (profilin-P_{10}), characterized by equilibrium dissociation constants, K_1^{diss} and K_2^{diss}, respectively; binding of a second molecule of profilin to the previously unoccupied polyproline tract then results in a doubly occupied complex, $\mathbf{P_2EE'}$, characterized by two equilibrium dissociation constants, $\alpha K_1^{diss} (= K_3^{diss})$ and

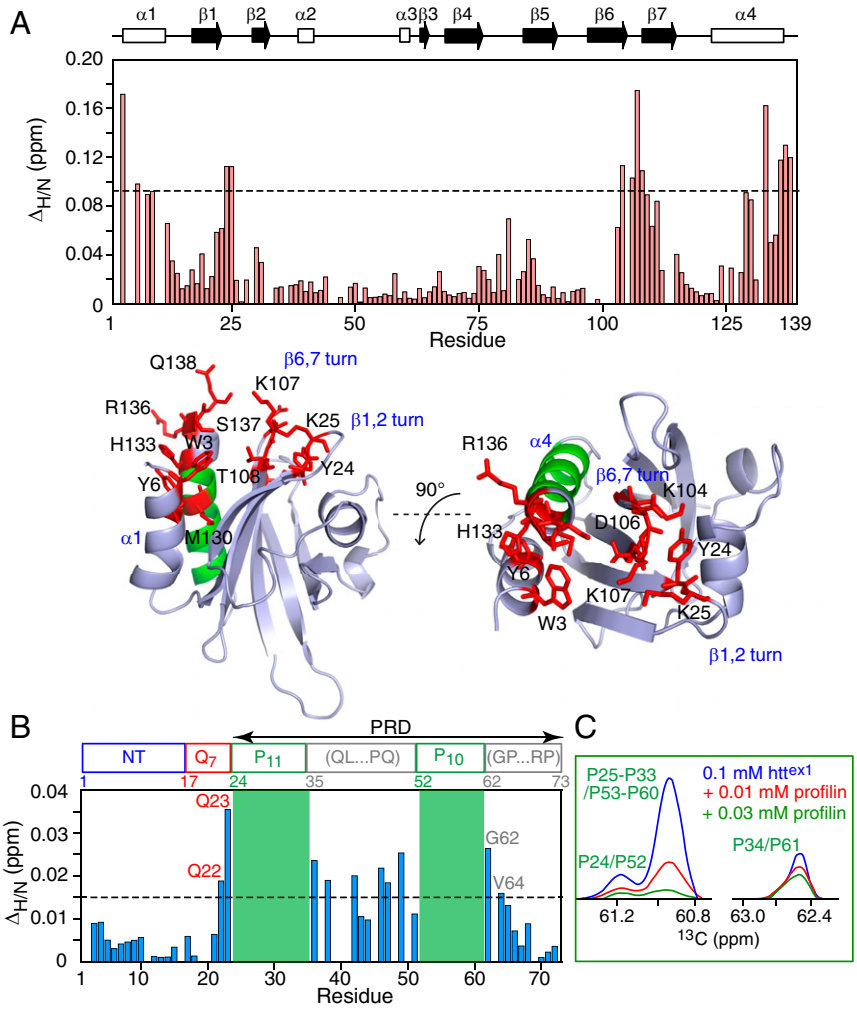

Fig. 3. $^{1}H_N/^{15}N$ chemical shift perturbation mapping of the profilin–htt^{ex1} binding interface. Weighted $^{1}H_N/^{15}N$ chemical shift perturbation ($\Delta_{H/N}$) profiles measured on (*A*) 0.4 mM ^{15}N-labeled profilin in the presence of 0.9 mM unlabeled htt^{ex1} (*Top*) and (*B*) 0.1 mM ^{15}N-labeled htt^{ex1} in the presence of 0.8 mM unlabeled profilin. (As the backbone nitrogen of proline is not bonded to a proton, the two polyproline tracts, shaded in green, are not detectable in ^{1}H–^{15}N HSQC correlation maps.) The data were obtained from ^{1}H–^{15}N HSQC spectra recorded at 600 MHz and 5 °C. $\Delta_{H/N}$ is the weighted chemical shift difference (38) in parts per million given by $(\Delta\delta_H^2 + \Delta\delta_N^2/25)^{1/2}$, where $\Delta\delta_H$ and $\Delta\delta_N$ are the $^{1}H_N$ and ^{15}N chemical shift differences in parts per million observed between the ^{1}H–^{15}N HSQC spectra of the ^{15}N-labeled binding partner in the absence and presence of the unlabeled binding partner. A ribbon representation of the structure of human profilin I [PBD code: 1PFL (39)] is shown in *A* (*Bottom*), with the regions involved in htt^{ex1} binding ($\Delta_{H/N} > 0.09$ ppm) and oligomerization (α-helix α_4) shown in red and green, respectively. (*C*) Cross-section through the ^{13}C indirect dimension of a ^{1}H–^{13}C HSQC spectrum of 0.1 mM $^{15}N/^{13}C$-labeled htt^{ex1} in the presence of varying amounts of unlabeled profilin (0, 0.01, and 0.03 mM profilin in blue, red, and green, respectively) illustrating line broadening of the $^{1}H\alpha/^{13}C\alpha$ proline cross-peaks within the two polyproline tracts upon addition of profilin. Note that the $^{1}H\alpha/^{13}C\alpha$ cross-peaks of the N- and C-terminal prolines are distinct from the other prolines, whose $^{1}H\alpha/^{13}C\alpha$ cross-peaks are completely overlapped (including the $^{1}H\alpha/^{13}C\alpha$ proline cross-peaks of the two polyproline tracts).

$\alpha K_2^{diss} = (K_4^{diss})$, where α is a cooperativity factor. The titration data for ^{15}N-labeled profilin report on all binding events since profilin contains only a single polyproline binding site (23), and the two polyproline tracts of htt^{ex1} differ by only a single proline in length. In the case of htt^{ex1}, however, binding of profilin to the two polyproline tracts can be monitored independently by making use of data from residues immediately preceding P_{11} (Gln22/Gln23) or following P_{10} (Gly62/Val65).

For all of the data used in the analysis of profilin–htt^{ex1} binding equilibria, exchange was assumed to be fast on the chemical shift timescale. For ^{15}N-labeled profilin, $\delta_{ex,i}$ for residue i as a function of unlabeled htt^{ex} concentration (c_{htt}) is given by $\delta_{ex,i}(c_{htt}) = \Delta\omega_i(p_{PE} + p_{PE'} + p_{P2EE'})$, where p_j is the fractional population of each of the complexes, and the chemical shift differences between free and bound profilin ($\Delta\omega_i$) are assumed to be the same for all complexes. For ^{15}N-labeled htt^{ex1}, $\delta_{ex,i}$ as a function of unlabeled profilin concentration (c_{prof}) is expressed by two separate relationships: $\delta_{ex,i}(c_{prof}) = \Delta\omega_i(p_{PE} + p_{P2EE'})$ for Gln22/Gln23 preceding the P_{11} tract and $\delta_{ex}(c_{prof}) = \Delta\omega_i(p_{PE'} + p_{P2EE'})$ for Gly62/Val65 following the P_{10} tract, respectively. In both instances, the chemical shifts of the doubly occupied species, $\mathbf{P_2EE'}$, are assumed to be the same as those of singly occupied ones ($\Delta\omega_{P2EE',i} = \Delta\omega_{PE,i}$ or $\Delta\omega_{P2EE',i} = \Delta\omega_{PE',i}$). The increase in the ^{15}N transverse relaxation rate, $^{15}N - \Delta R_2^{1.5kHz}$, where a 1.5-kHz spin-lock field is used to suppress line broadening arising from chemical exchange, arises from the substantial increase in molecular weight of the singly and doubly occupied complexes relative to free htt^{ex1}. In the fast exchange approximation, $^{15}N - \Delta R_{2,i}^{1.5kHz}(c_{prof})$ as a function of profilin concentration is given by $p_{PE}(R_{2,i}^{PE} - R_{2,i}^{E}) + p_{P2EE'}(R_{2,i}^{P2EE'} - R_{2,i}^{E})$ for Gln22/Gln23 and by $p_{PE'}(R_{2,i}^{PE'} - R_{2,i}^{E}) + p_{P2EE'}(R_{2,i}^{P2EE'} - R_{2,i}^{E})$ for Gly62/Val65, where $R_{2,i}^{E}$, $R_{2,i}^{PE}$, $R_{2,i}^{PE'}$, and $R_{2,i}^{P2EE'}$ are the transverse relaxation rates for residue i of free htt^{ex1}, the two singly occupied **PE** and **PE′**

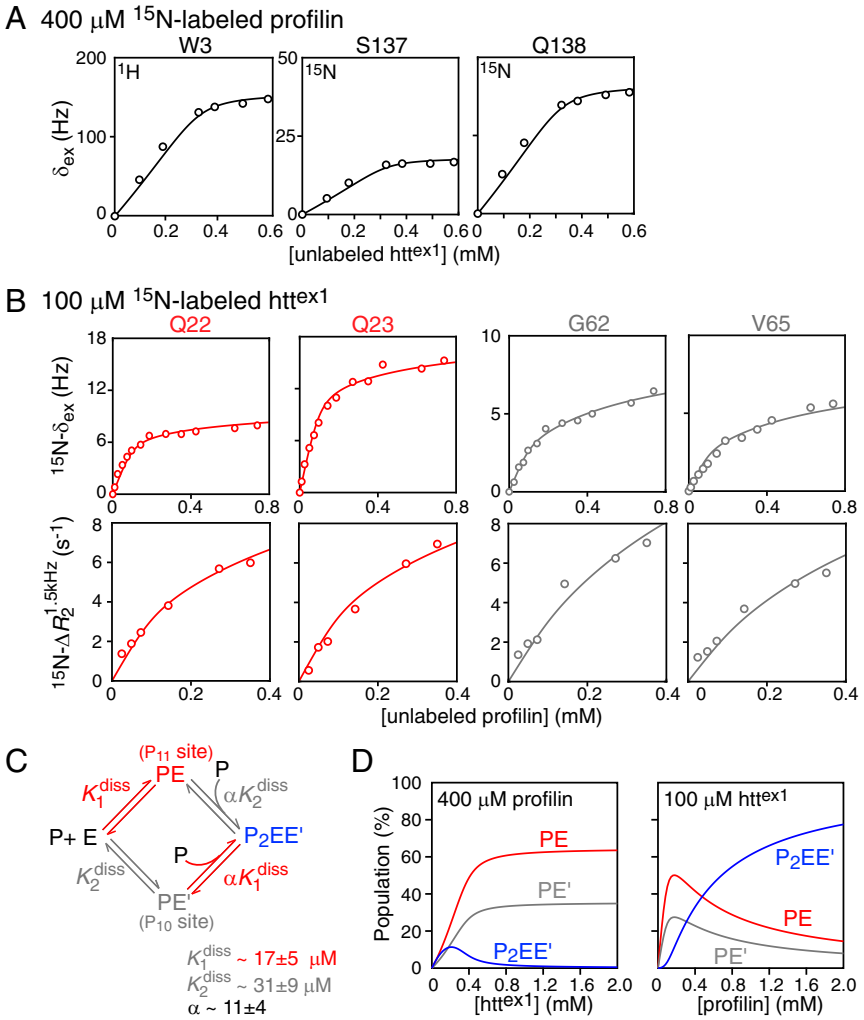

Fig. 4. Quantitative characterization of the binding equilibria involved in the interaction of profilin with htt^{ex1}. (*A*) Exchange-induced shifts for selected residues of 0.4 mM ^{15}N-labeled profilin upon titration with unlabeled htt^{ex1}. (*B*) Exchange-induced shifts, δ_{ex} (*Top* row) and $^{15}N - \Delta R_2^{1.5kHz}$ lifetime line broadening (*Bottom* row) for Gln22 and Gln23 (red; monitoring binding to P_{11}) and for Gly62 and Val65 (gray; monitoring binding to P_{10}) of 0.1 mM ^{15}N-labeled htt^{ex1} upon titration with unlabeled profilin. All experimental data were recorded at 600 MHz and 5 °C. (*C*) Scheme for the binding of profilin to the two polyproline tracts, P_{11} and P_{10}, of htt^{ex1}. The experimental data in *A* and *B* are shown by circles, and the best-fit curves from the global fit to the binding scheme shown in *C* are represented by solid lines. (*D*) Simulation of species' populations during the course of the titrations using the best-fit parameters for the equilibrium dissociation constants and cooperativity factor. For errors of 0.3 Hz and 0.6 s^{-1} for the δ_{ex} and R_2 data, the value of the reduced χ^2 is 0.81.

complexes, and the doubly occupied $\mathbf{P_2EE'}$ complex, respectively (see *SI Appendix*, Fig. S7, for validation of the fast exchange approximation in this instance). $R_{2,i}^{PE}$ and $R_{2,i}^{PE'}$ are assumed to be equal, and $R_{2,i}^{P2EE'}$ is scaled by a factor of 1.65 relative to $R_{2,i}^{PE}$ according to the ratio of the molecular weights of the doubly (~38 kDa) and singly (~23 kDa) occupied complexes. Further details of the fitting procedure are provided in *SI Appendix*, and the fitted values of the residue-specific parameters are given in *SI Appendix*, Table S2.

The equilibrium dissociation constants for the binding of profilin to the P_{11} and P_{10} polyproline tracts, K_1^{diss} and K_2^{diss}, obtained from the global fit, have values of 17 ± 5 and 31 ± 9 μM, respectively. The binding of the second profilin molecule to either of the P_{11} or P_{10} tracts (formation of the $\mathbf{P_2EE'}$ complex) is negatively cooperative with $\alpha = 11 \pm 4$. Since the linker connecting the P_{11} and P_{10} polyproline tracts is not excessively long (17 residues), negative cooperativity may possibly be attributed to partial occlusion of the second polyproline tract once the first polyproline tract is occupied by profilin.

The dependence of the fractional populations of the **PE**, **PE′**, and $\mathbf{P_2EE'}$ complexes on the total concentrations of profilin and htt^{ex1}, calculated using the experimental concentrations and the binding parameters obtained from the global fit, are shown in Fig. 4*D*. When 0.4 mM ^{15}N-labeled profilin is titrated with unlabeled htt^{ex1}, the population of the doubly occupied $\mathbf{P_2EE'}$ complex reaches a maximum at ~0.2 mM htt^{ex1}, and at the end of the concentration series (0.6 mM htt^{ex1}), $\mathbf{P_2EE'}$ is minimally populated and the predominant bound species are the two singly occupied complexes, **PE** and **PE′** (Fig. 4 *D*, *Left*). Given the relatively tight binding ($K_{1,2}^{diss}$ in the 15 to 30 μM range) of the first molecule of profilin to htt^{ex1}, these simulations explain why saturation is achieved close to 0.4 mM added htt^{ex1} (Fig. 4*A*). For the reverse titration, where unlabeled profilin is added to 0.1 mM ^{15}N-labeled htt^{ex1}, all three bound species are significantly populated (Fig. 4 *D*, *Right*) at the highest concentration (0.4 mM) of profilin employed in the experiments.

Kinetics of Profilin Binding to $\mathbf{htt^{NT}Q_7P_{11}K_2}$. To probe the kinetics of the interaction of profilin binding to the polyproline tracts of htt^{ex1}, we made use of a shorter construct, $htt^{NT}Q_7P_{11}K_2$ (Fig. 5*A*, and *SI Appendix*, Fig. S8), comprising only the first polyproline tract, P_{11}, followed by two lysines, as it would be problematic

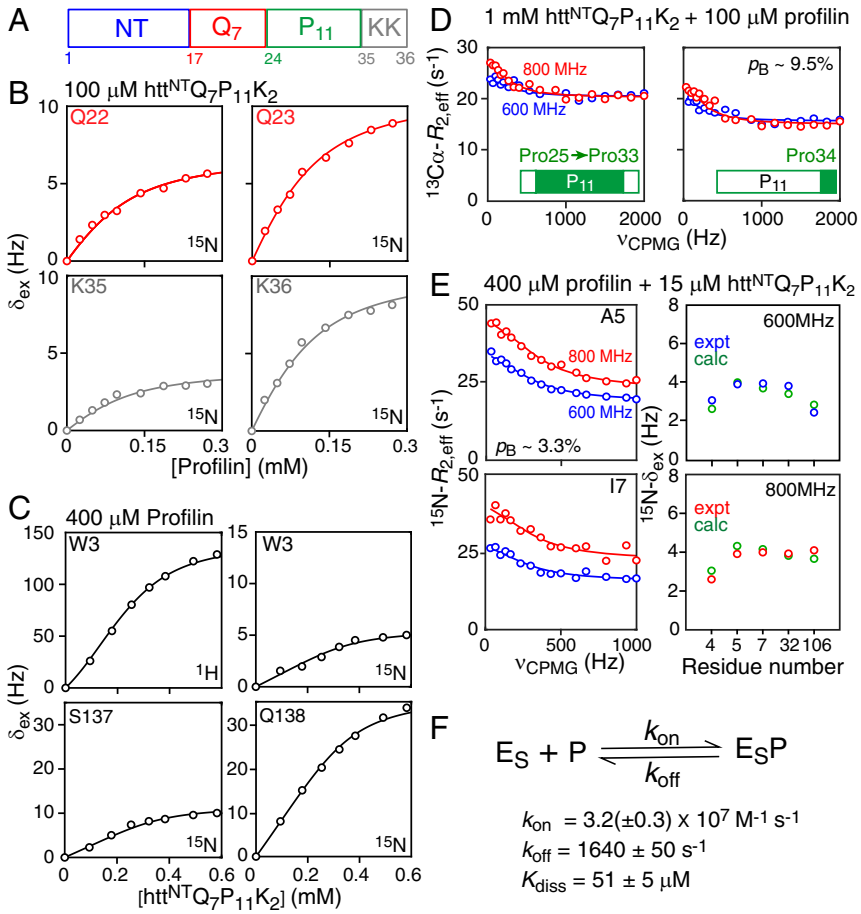

Fig. 5. Binding kinetics of the profilin–htt$^{NT}Q_7P_{11}K_2$ interaction. (*A*) Schematic representation of the htt$^{NT}Q_7P_{11}K_2$ domain architecture. (*B*) Exchange-induced ^{15}N shifts (δ_{ex}) at 600 MHz for residues immediately N-terminal (Gln22/Gln23, red) and C-terminal (Lys35/Lys36, gray) to the P_{11} polyproline tract observed for 0.1 mM $^{15}N/^{13}C\alpha$-labeled htt$^{NT}Q_7P_{11}K_2$ upon titration with unlabeled profilin. (*C*) Exchange-induced $^{1}H_N$ and ^{15}N shifts at 500 MHz observed for 0.4 mM $^{15}N/^{13}C$-labeled profilin upon titration with htt$^{NT}Q_7P_{11}K_2$. (*D*) $^{13}C\alpha$-CPMG relaxation dispersion profiles of the spectrally overlapped prolines (Pro25–Pro33) (*Left*) and the C-terminal proline (Pro34) (*Right*) of the P_{11} polyproline tract measured on 1 mM $^{15}N/^{13}C\alpha$-labeled htt$^{NT}Q_7P_{11}K_2$ in the presence of 0.1 mM unlabeled profilin at 600 (red) and 800 (blue) MHz. (*E*) ^{15}N-CPMG relaxation dispersion profiles (*Left*) and ^{15}N-δ_{ex} shifts (*Right*) measured on 0.4 mM $^{15}N/^{13}C$-labeled profilin in the presence of 15 μM htt$^{NT}Q_7P_{11}K_2$. All experimental data were recorded at 5 °C. (*F*) Kinetic scheme for the binding of profilin (P) to htt$^{NT}Q_7P_{11}K_2$ (E_S). The experimental data in *B*–*D* are shown as circles, and the best-fit curves to the kinetic scheme are shown as solid lines, with the exception of the best-fit ^{15}N-δ_{ex} values shown in *D*, which are shown as green circles. The population of the bound complex (p_B) for the observed species is indicated in *D* and *E*. For errors of 0.3 Hz, 2 Hz, and 0.6 s^{-1} for ^{15}N-δ_{ex}, $^{1}H_N$-δ_{ex}, and $^{15}N/^{13}C\alpha$ $R_{2,eff}$, respectively, the value of the reduced χ^2 is 2.56.

to determine the rate constants for the four-state binding scheme involving full-length htt^{ex1}. Global analysis was based on exchange-induced shifts observed on ^{15}N-labeled htt$^{NT}Q_7P_{11}K_2$ upon titration with unlabeled profilin (Fig. 5*B*), exchange-induced shifts observed on $^{15}N/^{13}C$-labeled profilin upon titration with unlabeled htt$^{NT}Q_7P_{11}K_2$ (Fig. 5*C*), $^{13}C\alpha$-CPMG relaxation dispersion profiles for the prolines of $^{15}N/^{13}C\alpha$-labeled htt$^{NT}Q_7P_{11}K_2$ in the presence of a small amount of unlabeled profilin (Fig. 5*D*), and ^{15}N-CPMG relaxation dispersion profiles and exchange-induced shifts for $^{15}N/^{13}C$-labeled profilin in the presence of a small amount of unlabeled htt$^{NT}Q_7P_{11}K_2$ (Fig. 5*E*). Of note, the residues of htt$^{NT}Q_7P_{11}K_2$ and profilin that exhibit exchange-induced shifts shown in Fig. 5 *B* and *C*, respectively, do not display any ^{15}N-CPMG relaxation dispersions (*SI Appendix*, Fig. S9 *A* and *B*); $^{13}C\alpha$-CPMG dispersion profiles, however, are observed for the polyproline tract of htt^{ex1} (Fig. 5*D*), and several residues of profilin also show ^{15}N-CPMG dispersions (Fig. 5*E* and *SI Appendix*, Fig. S9*C*). These exchange conditions benefit from combined analysis of relaxation dispersion and exchange-induced shift data (29). Details of the fitting procedure are provided in *SI Appendix*, and the best-fit values of the residue-specific parameters are listed in *SI Appendix*, Table S3.

The lifetime of the profilin–htt$^{NT}Q_7P_{11}K_2$ complex under the conditions of the CPMG relaxation dispersion experiments is ~600 μs with a K_{diss} value of ~51 μM. The association rate constant, k_{on}, is ~3 × 10^7 $M^{-1}{\cdot}s^{-1}$, consistent with a diffusion-limited reaction. The threefold weaker binding to the P_{11} polyproline tract of htt$^{NT}Q_7P_{11}K_2$ relative to that of htt^{ex1} may possibly be due to end effects: namely, the absence of the linker as well as the second P_{10} polyproline tract in htt$^{NT}Q_7P_{11}K_2$. The values of ^{15}N-Δω obtained from the global fits for the residues of htt$^{NT}Q_7P_{11}K_2$ and profilin that show ^{15}N exchange-induced shifts, but no ^{15}N-CPMG relaxation dispersions, are <0.6 ppm, while those residues of profilin that show ^{15}N-CPMG relaxation dispersions are in the range 1.3 to 2.8 ppm (*SI Appendix*, Table S3), explaining why the exchange process occurs in different regimes on the chemical shift timescale for these sites. The values of $|^{13}C\alpha$-$\Delta\omega|$ for Pro25–Pro33 and Pro34, obtained from the $^{13}C\alpha$-CPMG relaxation dispersion data, are ~0.3 ppm, and inspection of the corresponding cross-peaks in the ^{1}H–$^{13}C\alpha$ HSQC spectra of 1 mM htt$^{NT}Q_7P_{11}K_2$, in the absence and presence of 100 μM profilin (*SI Appendix*, Fig. S10), indicates that the exchange-induced shifts for the proline $^{1}H\alpha$ and $^{13}C\alpha$ nuclei are negative in sign, characteristic of a propensity toward PPII helix

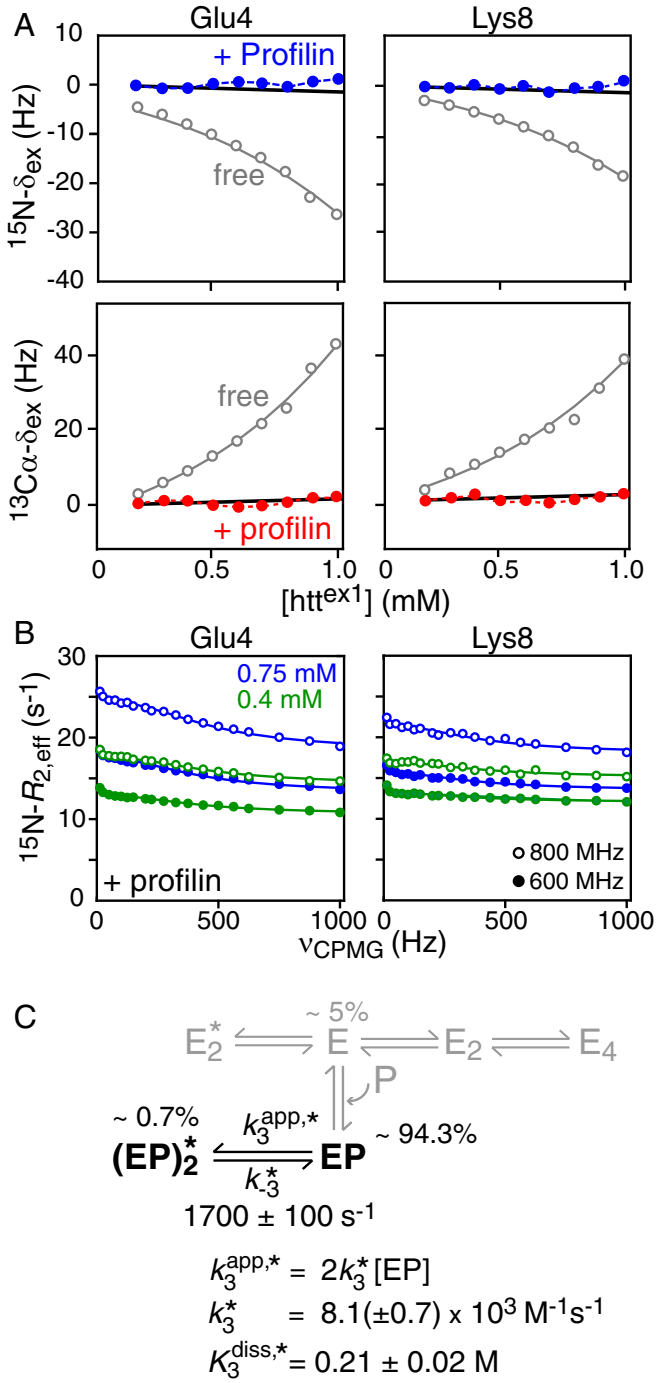

Fig. 6. Effect of profilin on prenucleation, transient oligomerization of the NT domain htt^{ex1}. (*A*) Concentration dependence of ^{15}N (*Top*, blue circles) and ^{13}Cα (*Bottom*, red circles) exchange-induced shifts of ^{15}N/^{13}Cα-labeled htt^{ex1} in the presence of 4.8 mM profilin (referenced relative to the shifts at 50 μM htt^{ex1}). The ^{15}N- and ^{13}Cα-δ_{ex} values obtained for htt^{ex1} in the absence of profilin are reproduced in gray from Fig. 2*B* for comparison. All measurements were performed at 800 MHz and 5 °C. (*B*) Examples of ^{15}N-CPMG relaxation dispersion profiles acquired at 600 (filled-in circles) and 800 (open circles) MHz and 5 °C on 0.4 (green) and 0.75 (blue) mM ^{15}N-labeled htt^{ex1} in the presence of 4.8 mM profilin. (*C*) Overall kinetic scheme for the oligomerization of htt^{ex1} bound to profilin (**EP**). (Note the singly and doubly bound species denoted as **PE**, **PE**′, and **P$_2$EE**′ in Fig. 2 are combined into a single species **EP** for the purpose of this analysis.) Only the off-pathway leading to the "nonproductive" $(\mathbf{EP})_2^*$ dimer remains active when profilin is bound. The population of free htt^{ex1} in the presence of 4.5 mM profilin is only 5%, and hence, the oligomeric species of free htt^{ex1} shown in gray, whose populations are <0.05%, do not make any measurable contribution to either the ^{15}N-CPMG relaxation dispersion profiles or the ^{15}N/^{13}Cα exchange-induced shifts. Furthermore, the residues analyzed, all of which are located in the NT domain, do not show changes in chemical shifts upon binding to profilin, and hence the binding of profilin to free htt^{ex1} does not contribute to the CPMG relaxation dispersions either. The species populations listed in the figure correspond to those at the highest concentration of htt^{ex1} used in ^{15}N-CPMG relaxation dispersion experiments (0.75 mM). The solid lines in *B* are the best-fit curves (reduced $\chi^2 = 0.77$ for errors of 0.3 s^{-1} for $R_{2,eff}$) obtained from global fitting of the ^{15}N-CPMG relaxation dispersion data to the two-state exchange system depicted in black in *C*. The thick black solid lines in *A* are the backcalculated ^{15}N (*Top*) and ^{13}Cα (*Bottom*) exchange-induced shifts for ^{15}N and ^{13}Cα Δω values of 2 and 3 ppm, respectively. The ^{15}N-Δω values were taken from the fits to the ^{15}N-CPMG relaxation dispersion data (*SI Appendix*, Table S4); in the case of ^{13}Cα-Δω, 3 ppm is comparable to the largest ^{13}Cα-Δω value observed for free htt^{ex1} (*SI Appendix*, Table S1).

formation (33). In addition, the very weak field dependence of the observed ^{15}N-δ_{ex} shifts for profilin in the presence of htt^{NT}Q$_7$P$_{11}$K$_2$ (right column in Fig. 5*E*) is fully consistent with the results of our analysis as explained in detail in *SI Appendix*, Fig. S11.

Extrapolation of the results of the kinetic study of htt^{NT}Q$_7$P$_{11}$K$_2$–profilin binding to full-length htt^{ex1}–profilin interactions, allows us to conclude that the interconversion between the free and bound species occurs on a moderately fast timescale ($\tau_{ex} \sim 600$ μs with $k_{ex} \geq 4\Delta\omega_N$ for the majority of htt^{ex1} or profilin sites), thus validating the approach used for analysis of htt^{ex1}–profilin binding equilibria.

On-Pathway Transient Oligomerization of htt^{ex1} Is Inhibited by Binding of Profilin. Thioflavin T assays on htt^{ex1} constructs containing up to a 40-residue polyglutamine tract have shown that addition of profilin reduces the rate of htt^{ex1} fibrillation (25). We hypothesized that binding of profilin to the polyproline tracts of htt^{ex1} also modulates prenucleation, transient oligomerization of the NT domain.

To test the above hypothesis we examined the concentration dependence of ^{15}N and ^{13}Cα exchange-induced shifts (from 50 μM to 1 mM) and ^{15}N-CPMG relaxation dispersions (at 0.4 and 0.75 mM) for htt^{ex1} in the presence of a fixed (4.8 mM) concentration of profilin, ensuring close to complete (~95%) saturation of htt^{ex1} with profilin. The large exchange-induced shifts seen in the absence of profilin are completely abolished in the presence of profilin (Fig. 6*A*). These data indicate that the on-pathway leading to the formation of a tetramer via a productive dimer is completely inhibited. ^{15}N-CPMG relaxation dispersion, however, for residues within the NT domain (which does not bind profilin) are still observed (Fig. 6*B* and *SI Appendix*, Fig. S12) and arise exclusively from off-pathway dimerization.

The impact of profilin on the kinetic scheme for htt^{ex1} oligomerization is summarized in Fig. 6*C*. In terms of analysis, the only exchange process that contributes to the ^{15}N-CPMG relaxation dispersions is the one between profilin-bound htt^{ex1} monomer **EP** and off-pathway $(\mathbf{EP})_2^*$ dimer. This is because the residues analyzed are located within the NT domain and do not show changes in chemical shifts upon binding to profilin; hence exchange between free and profilin-bound htt^{ex1} monomer (shown in gray in Fig. 6*C*) does not generate ^{15}N-CPMG dispersions. Furthermore, since htt^{ex1} is ~95% saturated with profilin, the populations of the free oligomeric species (shown in gray in Fig. 6*C*) will be too low (<0.05%) to make any measurable contribution to either the ^{15}N-CPMG relaxation dispersion profiles or the ^{15}N/^{13}Cα exchange-induced shifts.

Best fitting of the ^{15}N-CPMG relaxation dispersion data (see *SI Appendix* for details) reveals that the overall interconversion rate ($\tau_{ex} \sim 600$ μs) between the profilin-bound htt^{ex1} monomer, **EP**, and the profilin-bound off-pathway dimer, $(\mathbf{EP})_2^*$, is comparable to that in the absence of profilin ($\tau_{ex} \sim 750$ μs; Fig. 2*C*). The equilibrium dissociation constant ($K_3^{diss,*} \sim 0.2$ M) for the

off-pathway $(\mathbf{EP})_2^*$ dimer is also largely unaffected by binding of profilin. The backcalculated ^{15}N- and ^{13}Cα exchange-induced shifts (thick black lines in Fig. 6*A*) expected for Δω values of 2 and 3 ppm, respectively, at 800 MHz are too small to be experimentally measurable over the 50 μM to 1 mM concentration range studied. The $|^{15}\text{N-}\Delta\omega|$ values for $(\mathbf{EP})_2^*$ are ∼2 ppm (*SI Appendix*, Table S4), about twofold larger than the corresponding values in the absence of profilin (*SI Appendix*, Table S1), possibly suggesting that the ensemble of partially helical states for the off-pathway $(\mathbf{EP})_2^*$ dimer may be somewhat more ordered in the presence of profilin.

Concluding Remarks. We have investigated the impact of human profilin I on the prenucleation, transient oligomerization events involving the full-length exon 1 huntingtin protein, htt^{ex1}, comprising the N-terminal oligomerization domain (NT), a short seven-residue polyglutamine tract, and a polyproline rich domain (PRD) containing two polyproline tracts. We show that when at least one profilin molecule is bound to the PRD of htt^{ex1}, the on-pathway (productive) oligomerization pathway, leading to the formation of a transient, helical coiled-coil tetramer of the NT domain, is effectively abolished, and only the off-pathway leading to a nonproductive, partially helical NT dimer (that does not oligomerize further) is preserved (Fig. 6*C*). This result provides a clear mechanism whereby binding of profilin to the PRD inhibits fibrillation and subsequent aggregation and toxicity of htt^{ex1} (23–25). Furthermore, the fact that the on-pathway for early-stage oligomerization of htt^{ex1} is eliminated by profilin, validates the branched oligomerization scheme first proposed for the shorter htt^{NT}Q$_7$ construct (26). Indeed, it is difficult to conceive a mechanism whereby the absence of an off-pathway leading to a nonproductive dimer of htt^{ex1} would be possible if only the latter is retained in the profilin–htt^{ex1} complex.

The above seemingly simple result required nonetheless a considerable amount of auxiliary investigations aimed at a quantitative description of transient oligomerization of the free (unliganded) full-length htt^{ex1}, as well as the binding equilibria and kinetics of htt^{ex1}–profilin interactions. First, using a combination of the state-of-the-art NMR techniques for the characterization of chemical exchange and binding equilibria, including CPMG relaxation dispersion, exchange-induced chemical shifts, and lifetime line broadening, we quantitatively characterized the impact of the C-terminal PRD domain, absent from the shorter huntingtin variant htt^{NT}Q$_7$ studied earlier (26), on the prenucleation transient, oligomerization events involving free htt^{ex1}. We found that, although the equilibrium dissociation constant of htt^{ex1} tetramers into on-pathway (productive) dimers (Fig. 2*C*) is preserved between the shorter and full-length huntingtin exon 1 variants, the presence of the PRD in full-length htt^{ex1} somewhat stabilizes both on- and off-pathway dimeric species relative to the monomer. Second, we quantitatively described the equilibria involved in the binding of profilin to the two distinct polyproline tracts, P$_{11}$ and P$_{10}$, within the PRD using a four-state binding model. The equilibrium dissociation constants for the binding of the first molecule of profilin are in the 15 to 30 μM range, but binding of a second profilin molecule is ∼11-fold weaker, indicative of negative cooperativity, possibly due to partial steric hindrance between spatially close profilin molecules. In this regard, we note that the intracellular concentration of profilin ranges from 10 to 40 μM (34), while that for huntingtin within whole brain is around 0.15 μM (35) and the estimated concentration of soluble htt^{ex1} fragments within neuronal inclusion bodies is ∼10 μM (15). Hence, significant occupancy of profilin bound to htt^{ex1} can be achieved in vivo. The kinetics of profilin binding were investigated using a shorter huntingtin construct containing only a single polyproline tract. Exchange between the free proteins and the complex occurs on a moderately fast timescale ($\tau_{ex} \sim 600$ μs) relative to the observed chemical shift changes upon binding.

Building upon the quantitative information on the early stages of htt^{ex1} oligomerization as well as profilin–htt^{ex1} interactions, we were able to unambiguously demonstrate that early-stage on-pathway oligomerization events in the aggregation of htt^{ex1} leading to tetramer formation are abrogated by binding of profilin to the polyproline tracts. Since the PRD does not participate directly in the intermolecular interactions that stabilize the on-pathway dimer and tetramer formed by the NT domain (26), how does profilin binding exert its inhibitory effect? A possible explanation may lie in steric hindrance from the relatively large profilin significantly reducing the probability of forming the site-specific contacts required to form the on-pathway helical coil-coiled dimer and tetramer; the off-pathway dimer, however, does not appear to constitute a single structure but an ensemble of conformations with different registers and degrees of overlap (26), and hence the formation of the off-pathway dimer is only minimally impeded by profilin binding.

Experimental Methods

A detailed description of expression, purification, and isotope labeling of htt^{ex1} and human profilin I, experimental details of NMR and analytical ultracentrifugation measurements, and details of all global data fitting procedures are provided in *SI Appendix*.

Data Availability Statement. All experimental relaxation dispersion, exchange-induced shift, and transverse relaxation data discussed in this paper are provided either in the main text or *SI Appendix*. The experimental data in digital format, together with MatLab scripts used in global fitting, have been deposited on Figshare (DOI: 10.6084/m9.figshare.11887860). In addition, the backbone chemical shifts for htt^{ex1} have been deposited in the Biological Magnetic Resonance Data Bank (36).

ACKNOWLEDGMENTS. We thank Drs. Enrico Rennella and Lewis E. Kay (University of Toronto) for providing backbone chemical shift assignments of human profilin I. We acknowledge the technical assistance of Drs. Dusty Baber, Dan Garrett, and Jinfa Ying (National Institute of Diabetes and Digestive and Kidney Diseases, NIH). This work was supported by the Intramural Program of the National Institute of Diabetes and Digestive and Kidney Diseases, NIH (to G.M.C., DK029023-19).

1. J. M. Andresen *et al.*; US–Venezuela Collaborative Research Group; HD MAPS Collaborative Research Group, The relationship between CAG repeat length and age of onset differs for Huntington's disease patients with juvenile onset or adult onset. *Ann. Hum. Genet.* **71**, 295–301 (2007).
2. G. P. Bates *et al.*, Huntington disease. *Nat. Rev. Dis. Primers* **1**, 15005 (2015).
3. T. Ratovitski *et al.*, Mutant huntingtin N-terminal fragments of specific size mediate aggregation and toxicity in neuronal cells. *J. Biol. Chem.* **284**, 10855–10867 (2009).
4. A. Neueder *et al.*, The pathogenic exon 1 HTT protein is produced by incomplete splicing in Huntington's disease patients. *Sci. Rep.* **7**, 1307 (2017).
5. B. A. Barbaro *et al.*, Comparative study of naturally occurring huntingtin fragments in *Drosophila* points to exon 1 as the most pathogenic species in Huntington's disease. *Hum. Mol. Genet.* **24**, 913–925 (2015).
6. W. C. Duim, Y. Jiang, K. Shen, J. Frydman, W. E. Moerner, Super-resolution fluorescence of huntingtin reveals growth of globular species into short fibers and coexistence of distinct aggregates. *ACS Chem. Biol.* **9**, 2767–2778 (2014).
7. E. Scherzinger *et al.*, Self-assembly of polyglutamine-containing huntingtin fragments into amyloid-like fibrils: Implications for Huntington's disease pathology. *Proc. Natl. Acad. Sci. U.S.A.* **96**, 4604–4609 (1999).
8. F. Saudou, S. Humbert, The biology of huntingtin. *Neuron* **89**, 910–926 (2016).
9. C. L. Hoop *et al.*, Polyglutamine amyloid core boundaries and flanking domain dynamics in huntingtin fragment fibrils determined by solid-state nuclear magnetic resonance. *Biochemistry* **53**, 6653–6666 (2014).
10. J. M. Isas, R. Langen, A. B. Siemer, Solid-state nuclear magnetic resonance on the static and dynamic domains of huntingtin exon-1 fibrils. *Biochemistry* **54**, 3942–3949 (2015).
11. C. L. Hoop *et al.*, Huntingtin exon 1 fibrils feature an interdigitated β-hairpin-based polyglutamine core. *Proc. Natl. Acad. Sci. U.S.A.* **113**, 1546–1551 (2016).
12. H. K. Lin *et al.*, Fibril polymorphism affects immobilized non-amyloid flanking domains of huntingtin exon1 rather than its polyglutamine core. *Nat. Commun.* **8**, 15462 (2017).
13. A. K. Thakur *et al.*, Polyglutamine disruption of the huntingtin exon 1 N terminus triggers a complex aggregation mechanism. *Nat. Struct. Mol. Biol.* **16**, 380–389 (2009).

14. S. L. Crick, K. M. Ruff, K. Garai, C. Frieden, R. V. Pappu, Unmasking the roles of N- and C-terminal flanking sequences from exon 1 of huntingtin as modulators of polyglutamine aggregation. *Proc. Natl. Acad. Sci. U.S.A.* **110**, 20075–20080 (2013).
15. M. Chen, P. G. Wolynes, Aggregation landscapes of Huntingtin exon 1 protein fragments and the critical repeat length for the onset of Huntington's disease. *Proc. Natl. Acad. Sci. U.S.A.* **114**, 4406–4411 (2017).
16. A. Ceccon *et al*., Interaction of huntingtin exon-1 peptides with lipid-based micellar nanoparticles probed by solution NMR and Q-band pulsed EPR. *J. Am. Chem. Soc.* **140**, 6199–6202 (2018).
17. D. E. Ehrnhoefer, L. Sutton, M. R. Hayden, Small changes, big impact: Posttranslational modifications and function of huntingtin in Huntington disease. *Neuroscientist* **17**, 475–492 (2011).
18. C. Cariulo *et al*., Phosphorylation of huntingtin at residue T3 is decreased in Huntington's disease and modulates mutant huntingtin protein conformation. *Proc. Natl. Acad. Sci. U.S.A.* **114**, E10809–E10818 (2017).
19. A. Ceccon, V. Tugarinov, G. M. Clore, TiO_2 nanoparticles catalyze oxidation of huntingtin exon 1-derived peptides impeding aggregation: A quantitative NMR study of binding and kinetics. *J. Am. Chem. Soc.* **141**, 94–97 (2019).
20. J. P. Miller, R. E. Hughes, "Protein interactions and target discovery in Huntington's disease" in *Neurobiology of Huntington's Disease: Applications to Drug Discovery*, D. C. Lo, R. E. Hughes, Eds. (CRC Press, Boca Raton, FL, 2011), chap. 3.
21. A. Bochicchio, G. Rossetti, O. Tabarrini, S. Kraυβ, P. Carloni, Molecular view of ligands specificity for CAG repeats in anti-Huntington therapy. *J. Chem. Theory Comput.* **11**, 4911–4922 (2015).
22. L. M. Machesky, T. D. Poland, Profilin as a potential mediator of membrane-cytoskeleton communication. *Trends Cell Biol.* **3**, 381–385 (1993).
23. N. M. Mahoney, D. A. Rozwarski, E. Fedorov, A. A. Fedorov, S. C. Almo, Profilin binds proline-rich ligands in two distinct amide backbone orientations. *Nat. Struct. Biol.* **6**, 666–671 (1999).
24. J. Shao, W. J. Welch, N. A. Diprospero, M. I. Diamond, Phosphorylation of profilin by ROCK1 regulates polyglutamine aggregation. *Mol. Cell. Biol.* **28**, 5196–5208 (2008).
25. A. E. Posey *et al*., Profilin reduces aggregation and phase separation of huntingtin N-terminal fragments by preferentially binding to soluble monomers and oligomers. *J. Biol. Chem.* **293**, 3734–3746 (2018).
26. S. A. Kotler *et al*., Probing initial transient oligomerization events facilitating Huntingtin fibril nucleation at atomic resolution by relaxation-based NMR. *Proc. Natl. Acad. Sci. U.S.A.* **116**, 3562–3571 (2019).
27. A. G. Palmer, 3rd, NMR characterization of the dynamics of biomacromolecules. *Chem. Rev.* **104**, 3623–3640 (2004).
28. A. Mittermaier, L. E. Kay, New tools provide new insights in NMR studies of protein dynamics. *Science* **312**, 224–228 (2006).
29. P. Vallurupalli, G. Bouvignies, L. E. Kay, Increasing the exchange time-scale that can be probed by CPMG relaxation dispersion NMR. *J. Phys. Chem. B* **115**, 14891–14900 (2011).
30. S. J. Archer, V. K. Vinson, T. D. Pollard, D. A. Torchia, Elucidation of the poly-L-proline binding site in Acanthamoeba profilin I by NMR spectroscopy. *FEBS Lett.* **337**, 145–151 (1994).
31. W. J. Metzler, A. J. Bell, E. Ernst, T. B. Lavoie, L. Mueller, Identification of the poly-L-proline-binding site on human profilin. *J. Biol. Chem.* **269**, 4620–4625 (1994).
32. E. Rennella, A. Sekhar, L. E. Kay, Self-assembly of human profilin-1 detected by Carr-Purcell-Meiboom-Gill nuclear magnetic resonance (CPMG NMR) spectroscopy. *Biochemistry* **56**, 692–703 (2017).
33. M. A. Treviño *et al*., The singular NMR fingerprint of a polyproline II helical bundle. *J. Am. Chem. Soc.* **140**, 16988–17000 (2018).
34. S. H. Zigmond, Beginning and ending an actin filament: Control at the barbed end. *Curr. Top. Dev. Biol.* **63**, 145–188 (2004).
35. D. Macdonald *et al*., Quantification assays for total and polyglutamine-expanded huntingtin proteins. *PLoS One* **9**, e96854 (2014).
36. A. Ceccon, V. Tugarinov, G. M. Clore, Backbone ^{1}H, ^{13}C and ^{15}N chemical shift assignments for full length exon-1 huntingtin protein. Biological Magnetic Resonance Data Bank. http://www.bmrb.wisc.edu/data_library/summary/index.php?bmrbid=50122. Deposited 12 December 2019.
37. T. R. Alderson, J. H. Lee, C. Charlier, J. Ying, A. Bax, Propensity for *cis*-proline formation in unfolded proteins. *ChemBioChem* **19**, 37–42 (2018).
38. S. Grzesiek, S. J. Stahl, P. T. Wingfield, A. Bax, The CD4 determinant for downregulation by HIV-1 Nef directly binds to Nef. Mapping of the Nef binding surface by NMR. *Biochemistry* **35**, 10256–10261 (1996).
39. W. J. Metzler *et al*., Refined solution structure of human profilin I. *Protein Sci.* **4**, 450–459 (1995).